IOP Conf. Series: Materials Science and Engineering **149** (2016) 012173 doi:10.1088/1757-899X/149/1/012173

Mixed-state ferromagnetism in cubic Ni/ZrO_2 nanocomposites by microwave combustion synthesis

Tapas R Sahoo*, Sirish R Panda and Pragyan P Rath

Department of Chemistry, School of Applied Sciences, KIIT University, Bhubaneswar, Odisha, India

E-mail: tapasji@gmail.com

This article shows the magnetic phase diagram for $Zr_{1-x}Ni_xO_2$ compositions synthesized by microwave combustion method. The samples show room temperature ferromagnetism over the entire range of Ni-doping. Ni^{2+}/ZrO_2 (<4 at% Ni) indicates a safe substitution limit to show dilute magnetic phase. There is a threshold limit to this Dilute Magnetic Semiconductor (DMS) phase up to ~ 4%, above which this system serves as a model system for cluster induced magnetism. Microwave combustion method is a convenient and an inexpensive approach to evaluate magnetism in these high temperature phases, which is otherwise possible only by Physical vapor deposition techniques.

1. Introduction

Oxide-diluted magnetic semiconductors (O-DMS) [1] have attracted a great deal of interest in recent years due to the possibility of inducing room temperature ferromagnetism. These materials are of particular interest due to the projected applications in spintronics [2, 3] and potentially new mechanisms of ferromagnetism (FM) [4]. The presence of carriers is also an important consideration along with obtaining Curie temperature above room temperature to use these materials for practical applications. Titanium, Zirconium and Hafnium all belong to the same group IV (B) in the periodic table and their oxides Titania (TiO_2), Zirconia (ZrO_2) and Hafnia (HfO_2) have band gaps of 3.2 eV, 5.5 eV and 4.5 eV respectively. The discovery of room temperature ferromagnetism (FM) in a Co-doped anatase TiO_2 by Matsumoto *et al.* [5] and recent intriguing reports [6,7] on the observation of unexpected and highly anisotropic ferromagnetism in a high *k* dielectric oxide HfO_2 [8] have triggered considerable interest from the dilute magnetic semiconductors (DMS) community.

In this work, we have explored the possibility of occurrence of room temperature ferromagnetism in dilute phases of Ni-doped ZrO_2 samples, synthesized by doping different concentrations of Nickel. Interestingly, the high-*k* dielectric oxides such as ZrO_2 are already under active consideration as gate dielectrics for next generation devices in semiconductor technology in view of the material compatibility with Silicon. Introducing a magnetic response in such dielectrics should enable an integration of complementary metal-oxide semiconductor (CMOS) with spintronic technology. Moreover, in the wake of recent spur in research activity in DMS system [9], this work could throw light on the understanding of the underlying mechanism of the intriguing DMS behavior. We observe exceptionally strong room temperature ferromagnetic signal with very low percentage of Ni-doped ZrO_2, less than 4 at% Ni, which challenges our understanding of magnetism in wide band gap oxides because neither Zr^{4+} nor O^{2-} are magnetic ions and the d-shell of the Zr^{4+} ion is either empty or full. In general, ferromagnetic insulators (FI) are rare since in insulating compounds, spins tend to couple with each other antiferromagnetically. With light shed from the resulting research on introducing room temperature ferromagnetism by doping transition metals into different wide band gap oxides such as TiO_2 [10-14], and HfO_2 [15-18], we undertook an investigation of doping Nickel (and other 3d ferromagnetic metals) in ZrO_2, to verify if such a doping can result in magnetic semiconducting matrix.

Several different methods have been investigated as routes for the synthesis of zirconia nanoparticles, which include the sol-gel process [19], spray pyrolysis [20], mechanochemical

Content from this work may be used under the terms of the Creative Commons Attribution 3.0 licence. Any further distribution of this work must maintain attribution to the author(s) and the title of the work, journal citation and DOI.
Published under licence by IOP Publishing Ltd

processing [21], emulsion precipitation [22] etc. However, most of these methods use alkoxide as raw material, which is too expensive to be used in a large-scale production. Among the various solution routes employed for the preparation of oxide materials, the solution combustion process seems to be a versatile one. This method is quite simple, does not involve multiple steps and yields high surface area products of desired composition and structure which are sinter active. Being a solution process, atomic level doping and homogeneity can be achieved. Here, we have synthesized high temperature cubic phase zirconia, without any additives as stabilizing agent, via wet combustion route. The present work addresses the preparation of a series of Ni-ZrO_2 CERMET nanocomposites that possess superior magnetic properties and discusses the effect of the dispersion of nickel particles on the magnetic properties of the Ni/ZrO_2 composite system.

2. Experimental

Microwave assisted combustion synthesis was employed to synthesize ZrO_2 and Ni-doped ZrO_2 compositions [23, 24], which stabilizes high temperature metastable cubic phase of ZrO_2. In a typical reaction, stoichiometric amounts of analytical grade of 1g. Zirconyl Nitrate ($ZrO(NO_3)_2$) was mixed with 0.1397g, 0.3144g, 0.539g & 0.8384g of Nickel Nitrate ($Ni(NO_3)_2$) for $Zr_{0.9}Ni_{0.1}O_2$, $Zr_{0.8}Ni_{0.2}O_2$, $Zr_{0.7}Ni_{0.3}O_2$ & $Zr_{0.6}Ni_{0.4}O_2$ compositions respectively, in minimum amount of distilled water in a 100 ml beaker. A corresponding amount of 0.529g, 0.5951g, 0.6801g & 0.7935g of di-formal hydrazine (DFH) was added as dictated by the Oxidizer/Fuel (O/F) ratio [24]. The resulting mixture was exposed to microwave irradiation at high power of 800 W and frequency of 2450 MHz, for a maximum of 3 mins. This process is instantaneous and the resulting residue was powdery, foamy and X- ray crystalline. The ground samples were characterized by powder X-ray diffraction employing CuKα radiation. The magnetic properties were studied with a superconducting quantum interference device (SQUID) magnetometer. Magnetization (M) vs. applied magnetic field (H) measurement was compared with the measurements taken by Vibrating Sample Magnetometer (VSM). Temperature dependence of magnetization for as-prepared samples was measured at 1 Tesla field using SQUID. We show the high resolution transmission electron microscopy (HRTEM) and the selected area diffraction pattern (SAD) for the structural characterization of the samples.

3. Results and discussion

Solution combustion method provides a convenient route for the synthesis of $Zr_{1-x}Ni_xO_2$ solid solution. Figure 1.(a) & (b) show Rietveld refined powder XRD pattern for $Zr_{0.99}Ni_{0.01}O_2$ and $Zr_{0.96}Ni_{0.04}O_2$ respectively. This shows the formation of single phase products with the cubic fluorite structure. No peak of any secondary phase was seen in the spectra. This is noteworthy since conventional wet route synthesized ZrO_2 samples do not crystallize in cubic phase, as a result Yttria is added to stabilize cubic zirconia phase. Insets show the X-ray diffraction pattern of 1% & 4% Ni-doped ZrO_2. Lattice parameter 'a' is found to be 5.1128 for x = 0.01 and 5.1132 for x = 0.04.

Figure 2 shows the X-ray diffraction pattern, for higher Ni doped $Zr_{1-x}Ni_xO_2$ compositions ($0.0< x <0.6$), which crystallize in a cubic phase. The as-prepared samples do not show any impurity peaks up to 20% doping. Beyond 20% doping Ni metal and NiO impurity phases are observed. In 30% & 40% Ni composition, metallic Ni phase (JCPDS 04-0850) is observed. In 50% Ni composition, both Ni (marked by the #) and NiO (marked by the *) phases are observed. Whereas for 60% composition, only NiO peaks (JCPDS 75-0269) are observed with enhancement in intensity as compared to other compositions.

Magnetic properties of 1% & 4% Ni/ZrO_2 samples were characterized by a quantum design superconducting quantum interference device magnetometer (SQUID). In figure 3(a) & (b), we show the M–H loop for $Zr_{0.99}Ni_{0.01}O_2$ & $Zr_{0.96}Ni_{0.04}O_2$ recorded at 300K & 4.2K respectively. Hysteresis is observed, indicating clear evidence for ferromagnetism at room temperature. It can be seen that the samples show coercivity of about 110 Oe & 245 Oe for 1 at% Ni and 120 Oe & 265 Oe for 4 at% Ni sample at 300K & 4.2K respectively. The 1at% Ni sample attains saturation around 0.2 Tesla with a saturation magnetization of about 0.053 emu/g at 300K, whereas at 4.2K the sample does not apparently saturate up to a field of 1.75 T. For the 4at% Ni-doped sample the saturation occurs around

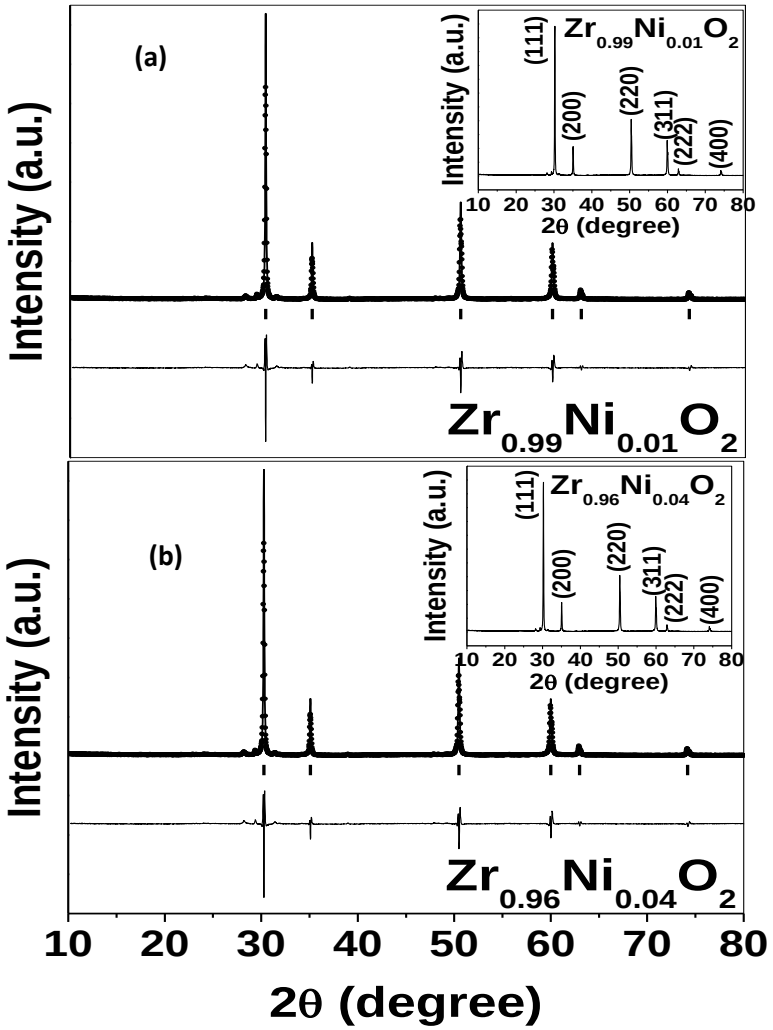

Figure 1. (a) Shows the Rietveld refined powder XRD pattern of $Zr_{0.99}Ni_{0.01}O_2$. Inset shows the X-ray diffraction pattern of 1at% Ni-doped ZrO_2 with the cubic fluorite structure. Figure 1(b) shows the Rietveld refined powder XRD data for $Zr_{0.96}Ni_{0.04}O_2$. Inset shows the X-ray diffraction pattern of 4 at% Ni-doped ZrO_2, without any evidence of secondary phase.

0.2 Tesla with a saturation magnetization of about 0.17 emu/g at 300K whereas again at 4.2K, the sample does not saturate up to a field of 1.75 T. Inset to figure 3(b) shows the M vs. H plot of the parent ZrO_2, showing a typical diamagnetic loop. This ensures that the ferromagnetism (FM) is because of Ni-doping only. From the plots it is clear that the samples are ferromagnetic at 300K whereas at 4.2K, there is a clear indication of a paramagnetic signal superimposed on the ferromagnetic signal. The magnetic particle size [25] can be calculated from the hysteresis curve. For an isotropic particle, the magnetic particle size,

$$d = (V)^{1/3} = [(6\mu) / (\pi M_s)]^{1/3} \qquad (1)$$

Where, 'M_s' is the bulk saturation magnetization of the material, 'μ' is the corresponding magnetic moment and 'V' is the volume of the particle. The effective magnetic particle size was calculated to be 1.63 nm and 1.62 nm and the magnetic moment per atom was found to be 0.0012 and 0.38μ_B for 1% and 4% Ni-doped ZrO_2 respectively.

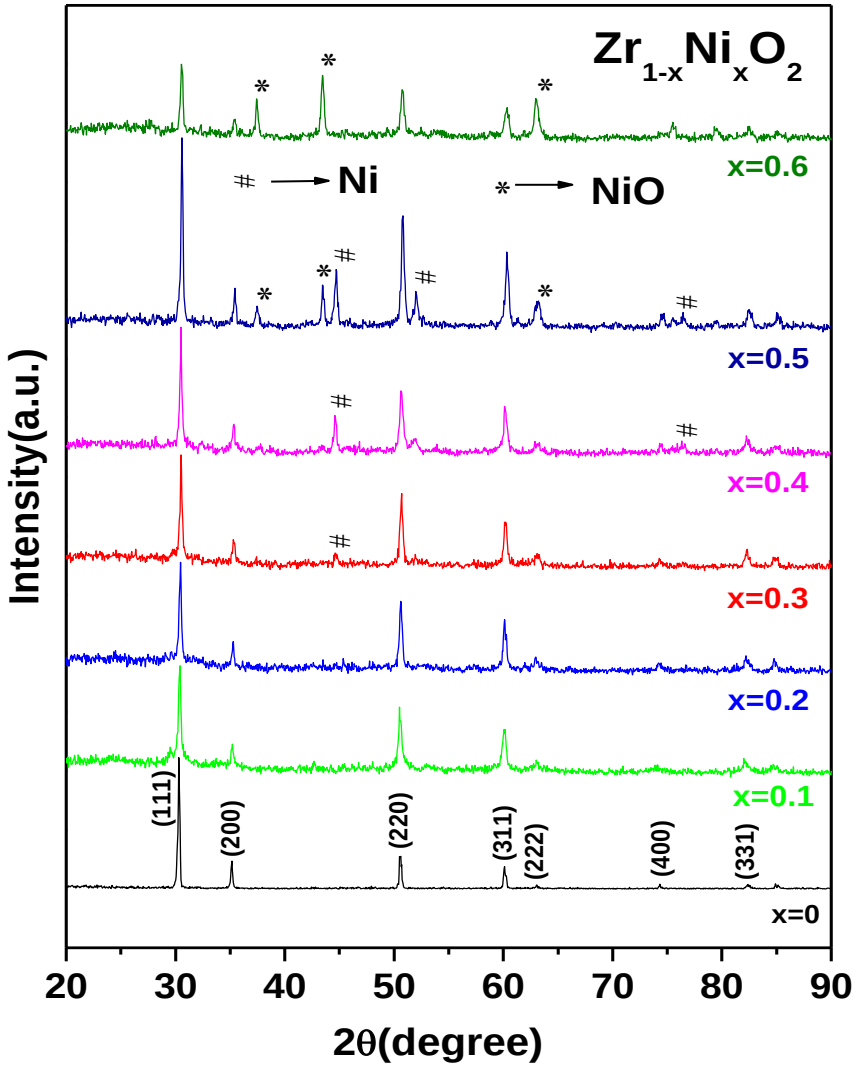

Figure 2. Shows the X-ray diffraction pattern of the as-prepared $Zr_{1-x}Ni_xO_2$ ($0 < x <$ 0.6) samples. Note that, the figure do not show any impurity peaks up to 20% doping and beyond 20% doping Ni metal & NiO impurity peaks are observed (marked by '#' & '*').

The small coercivities (110 Oe, 120 Oe at 300K) and the resulting small hysteresis characterize these materials as soft ferromagnets. There is a gradual decrease in H_c with increasing temperature, which is similar to the behavior observed in other magnetic systems such as Ni: ZnO [26] & transition metal (M = Co, Mn, Cr, Ni) doped ZnO [27] and is consistent with the thermally activated magnetization reversal. At 4.2K, the decrease in saturation magnetization in both the samples cannot be attributed to the paramagnetism of Ni^{2+} in ZrO_2 because, tetrahedral Ni^{2+} shows only temperature independent paramagnetism at low temperature. Instead, we attribute this temperature-dependent magnetization to superparamagnetism that stems from magnetic ordering in fused crystalline Ni^{2+}:ZrO_2 domains, too small to support long range FM.

The M vs. H hysteresis loops at room temperature is presented in figure 4, which shows a comparison of hysteresis loops with different percentage of Ni in cubic ZrO_2. The magnetic behavior shows increase in moment, with increase in Ni concentration. Figure 5 shows the variation of M_s with

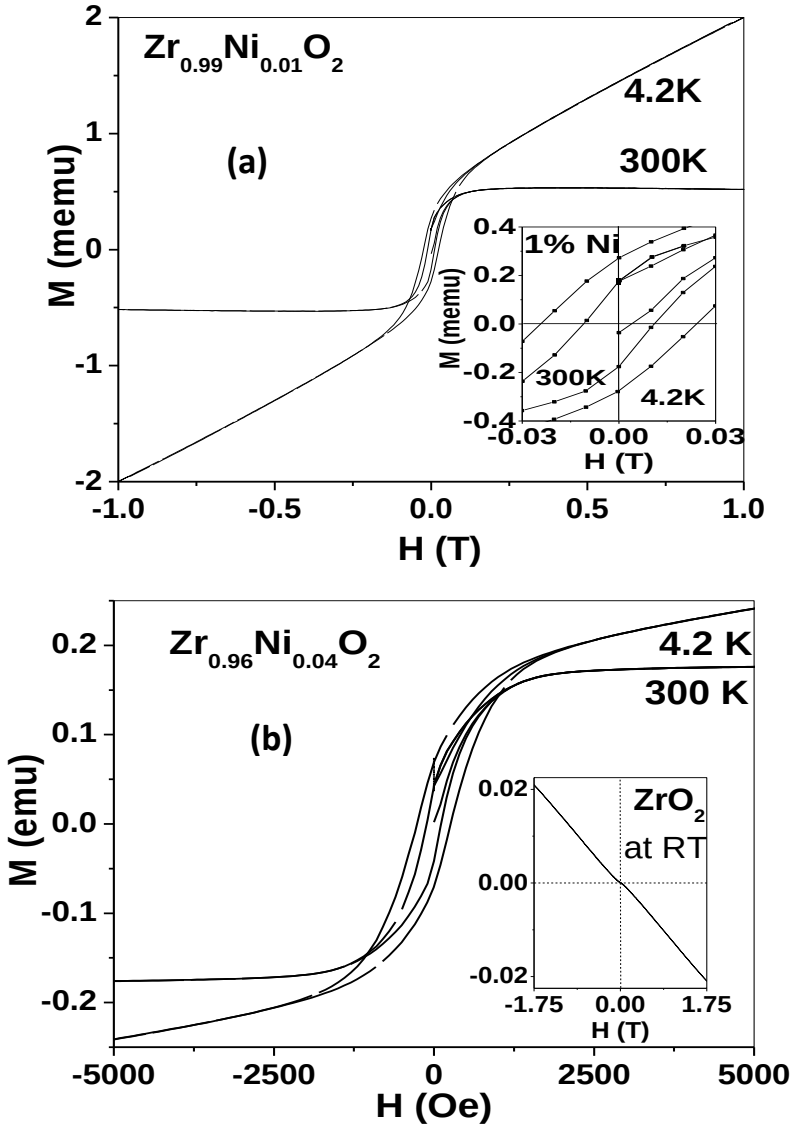

Figure 3. Shows the plot of Magnetization as a function of applied magnetic field of $Zr_{0.99}Ni_{0.01}O_2$ (a) & $Zr_{0.96}Ni_{0.04}O_2$ (b) at 300 K & 4 K respectively. The inset to (a) shows coercivities of about 110 Oe & 245 Oe for 1 at% Ni and inset to (b) shows the M vs. H plot of parent ZrO_2 at room temperature, this shows diamagnetic behavior.

Ni conc. Here we can see that the M_s value increases sharply for higher Ni compositions, i.e. in 20% - 50% range, beyond which it decreases. The major contribution to magnetization appears to be from metallic nickel clusters for compositions above 20% Ni, which is evident from the XRD pattern (figure 2) where we observe Ni metal peaks for 30, 40 & 50 %. And the rapid decrease in magnetization beyond 50% is due to the antiferromagnetic NiO phase.

In figure 6.(a), we further show the electron diffraction pattern, showing polycrystalline rings corresponding to the d-spacing of ZrO_2. For the 1at% Ni:ZrO_2 composition, no secondary phase was observed except for ZrO_2 phase, indicating that either Ni may be substituted at the Zr sites or Ni nano clusters are intimately coated by the ZrO_2 particles. However, for the 4at% composition, the appearance of NiO (figure 6.b) suggests the evidence for Ni substitution at the Zr sites, as there is

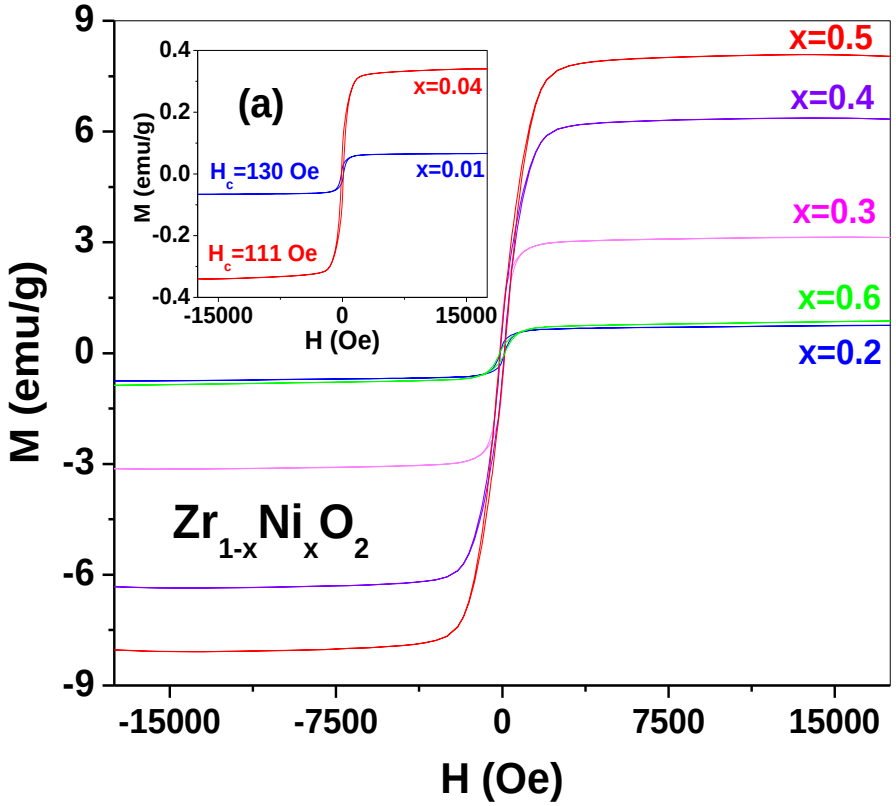

Figure 4. Shows the M vs. H measurements of Ni-doped ZrO_2 series ($0<x<0.6$) at room temperature. Inset (a) shows the M vs. H plot (VSM) of $Zr_{0.99}Ni_{0.01}O_2$ and $Zr_{0.96}Ni_{0.04}O_2$.

increase in magnetic moment with increase in Ni-doping. If such a Ni^{2+} state is correlated to NiO impurity phase, then magnetic moment has to decrease since NiO is anti-ferromagnetic. Figure 6.(c) shows a high resolution TEM image of 1% Ni-doped ZrO_2 bulk sample, revealing a well developed crystalline structure of $Zr_{0.99}Ni_{0.01}O_2$ nanoparticle embedded in a ZrO_2 matrix. The dimensions of nanoparticles ranged from 5 nm (inset to figure 6.c) to 14 nm (figure 6.d). This wide range of particle size distribution is expected because of different exothermicity produced during the combustion reaction, as a result of different fuel ratio and of different transition metal (Ni) compositions. In figure 7, we show evidence for the presence of Ni cluster and NiO phases from TEM micrographs which are

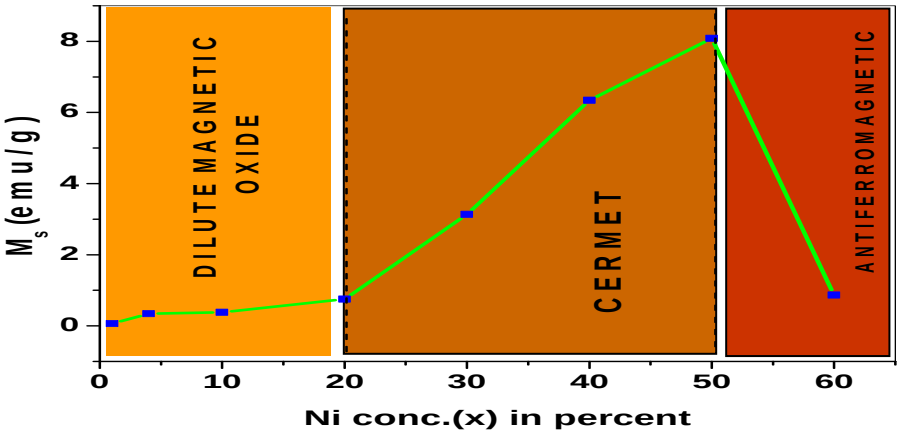

Figure 5. Shows the plot of variation of M_s with increase in Ni concentration.

in agreement with our XRD pattern. For 50 & 60%, we see signature for NiO appearing in the SAED pattern. The TEM morphologies clearly show NiO grains embedded in ZrO_2 matrix. However, we do not see such evidence for Ni clusters in 1 & 4 % doped samples, whose morphologies are different from that of 50 & 60 %.

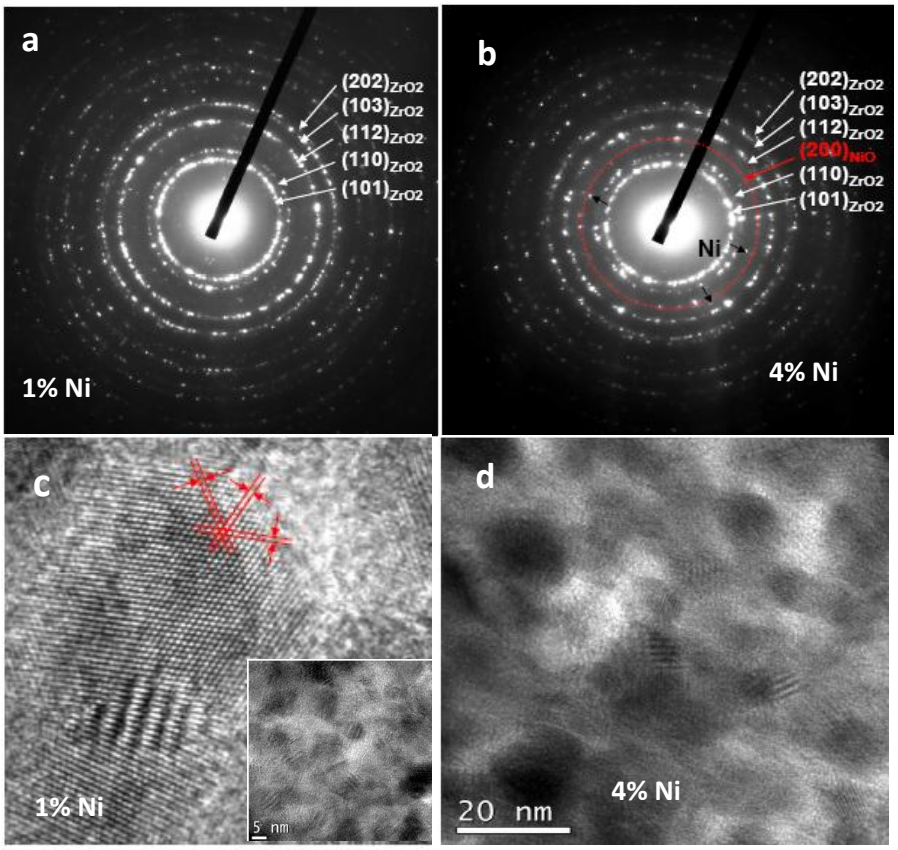

Figure 6. (a) & (b) show the Selected Area Electron Diffraction (SAED) patterns of 1 and 4 % Ni-doped ZrO_2. 6 (c) shows the High Resolution TEM image of 1% Ni and inset to (c) & (d) show TEM images of 1 & 4 % Ni respectively.

The absence of carriers and defects cannot stabilize dilute magnetic systems in the ferromagnetic state, provided the concentration of dopants is high to affect the overlap of the so-called bound magnetic polarons and not too high for antiferromagnetic exchange to dominate. In the present study on Ni-doped ZrO_2 samples both of these mechanisms are ruled out primarily due to the low dopant concentration. Moreover, Ni^{2+} energy levels are well within the band gap to eliminate the possibility of themselves providing any free carriers. Further we distinctly observe that the room temperature ferromagnetism (RTFM) even for 1at% Ni doped system wherein carrier induced ferromagnetism can be ruled out, which often results from hybridization of charge carriers with transition metal dopant ion. Further defect induced ferromagnetism can be ignored since ZrO_2 exists in the cubic phase and M_s increases with Ni concentration. Given these facts, it appears that the Ni/ZrO_2 provides a clear template for Ni^{2+} ion to substitute at the Zr sites, for low concentrations of Ni and for compositions from 20 - 50 at% Ni, a strong room temperature FM is observed, because of Ni metal cluster induced FM. Finally, we also mention that, for higher compositions of Ni, i.e. beyond 50 at%, a phase segregation of NiO precipitates, appear in the ZrO_2 matrix.

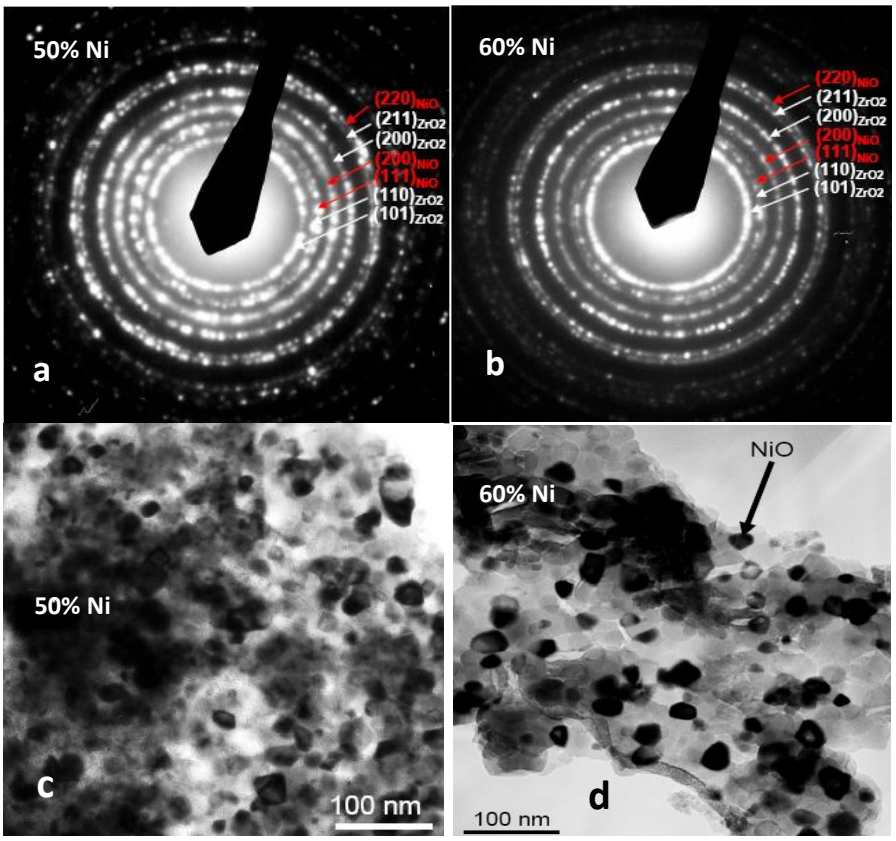

Figure 7. (a) & (b) show the SAED pattern of $Zr_{0.5}Ni_{0.5}O_2$ & $Zr_{0.6}Ni_{0.4}O_2$ and (c) & (d) show the TEM micrograph of $Zr_{0.5}Co_{0.5}O_2$ & $Zr_{0.6}Ni_{0.4}O_2$ respectively.

4. Summary

In summary, we have characterized the structural and magnetic properties of high quality Ni-doped ZrO_2 bulk samples synthesized by microwave combustion method. The samples show room temperature ferromagnetism over the entire doping concentration. Ni^{2+}:ZrO_2 (<4 at% Ni) indicates a safe substitution limit to show dilute magnetic phase. There is a safe compositional range, <4 at% Ni up to which there is likelihood for DMS, above which this system serves as a model system for cluster induced magnetism. Microwave combustion method is a convenient and an inexpensive approach to evaluate magnetism in high temperature phases, otherwise possible only by Physical vapor deposition techniques.

References

[1] Prellier W, Fouchet A and Mercey B 2003 *J. Phy.: Condens. Matter* **15** 1583.
[2] Prinz Gary A 1998 *Science* **282** 1660.
[3] Wolf S A, Awschalom D D, Buhrman R A, Daughton J M, Molnar S von, Roukes M L, Chtchelkanova A Y and Treger D M 2001 *Science* **294** 1488.
[4] Dietl T, Ohno H, Matsukura F, Cibert J and Ferrand D 2000 *Science* **287** 1019.
[5] Matsumoto Y, Murakami M, Shono T, Hasegawa T, Fukumura T, Kawasaki M, Ahmet P, Chikyow T, Koshihara S and Koinuma H 2001 *Science* **291** 854.
[6] Abraham D W, Frank M M and Guha S 2005 *Appl. Phys. Lett.* **87** 252502.
[7] Coey J M D, Venkatesan M, Stamenov P, Fitzgerald C B and Dorneles L S 2005 *Phys. Rev. B* **72** 024450.
[8] Venkatesan M, Fitzgerald C B and Coey J M D 2004 *Nature* **430** 630.
[9] Ohno H 1998 *Science* **281** 951.

[10] Zhang S X, Ogale S B, Fu L F, Dhar S, Kundaliya D C, Ramadan W, Browning N D and Venkatesan T 2006 *Appl. Phys. Lett.* **88**, 012513.
[11] Manivannan A, Glaspell G and Seehra M S 2003 *J. Appl. Phys.* **94** 6994.
[12] Fu L F, Browning N D, Zhang S X, Ogale S B, Kundaliya D C and Venkatesan T 2006 *J. Appl. Phys.* **100** 123910.
[13] Chen J, Rulis P, Ouyang L, Satpathy S and Ching W Y 2006 *Phys. Rev. B* **74** 235207.
[14] Chambers S A, Droubay T, Wang C M and Lea A S 2003 *Appl. Phys. Lett.* **82** 1257.
[15] Hong N H, Sakai J, Poirot N and Ruyter A 2005 *Appl. Phys. Lett.* **86** 242505.
[16] Hong N H, Poirot N and Sakai J 2006 *Appl. Phys. Lett.* **89** 042503.
[17] Rao M S R, Kundaliya D C, Ogale S B, Fu L F, Welz S J, Browning N D, Zaitsev V, Varughese B, Cardoso C A, Curtin A, Dhar S, Shinde S R, Venkatesan T, Lofland S E and Schwarz S A 2006 *Appl. Phys. Lett.* **88** 142505.
[18] Chang Y H, Soo Y L, Lee W C, Huang M L, Lee Y J, Weng S C, Sun W H, Hong M, Kwo J, Lee S F, Ablett J M and Kao C C 2007 *Appl. Phys. Lett.* **91** 082504.
[19] Moon Y T, Park H K, Kim D K and Kim C H 1995 *J. Am. Ceram. Soc.* **78** 2690.
[20] Stichert W and Schuth F 1998 *Chem Mater.* **10** 2020.
[21] McCormick P G, Tsuzuki T, Robinson J S and Ding J 2001 *Adv. Mater.* **13** 1008.
[22] Woudenberg F C M, Sager W F C, Sibelt N G M and Verweij H 2001 *Adv. Mater.* **13** 514.
[23] Manoharan S S, Swati, Prasanna S J, Rao M L and Sahu R K 2002 *J. Am.Ceram.Soc.***85** 2469.
[24] Manoharan S S and Patil K C 1992 *J. Am. Ceram. Soc.* **75** 12.
[25] An B H, Wu J H, Liu H L, Ko S P, Ju J S and Kim Y K 2008 *Colloids and Surfaces A:Physicochem. Eng. Aspects* **250** 313.
[26] Radovanovic P V and Gamelin D R 2003 *Phys. Rev. Lett.* **91** 157202.
[27] Ueda K, Tabata H and Kawai T 2001 *Appl. Phys. Lett.* **79** 988.